Membrane domain organization of myelinated axons requires βII spectrin

Chuansheng Zhang,[1] Keiichiro Susuki,[1] Daniel R. Zollinger,[1] Jeffrey L. Dupree,[2] and Matthew N. Rasband[1]

[1]Department of Neuroscience, Baylor College of Medicine, Houston, TX 77030
[2]Department of Anatomy and Neurobiology, Virginia Commonwealth University, Richmond, VA 23284

The precise and remarkable subdivision of myelinated axons into molecularly and functionally distinct membrane domains depends on axoglial junctions that function as barriers. However, the molecular basis of these barriers remains poorly understood. Here, we report that genetic ablation and loss of axonal βII spectrin eradicated the paranodal barrier that normally separates juxtaparanodal K^+ channel protein complexes located beneath the myelin sheath from Na^+ channels located at nodes of Ranvier. Surprisingly, the K^+ channels and their associated proteins redistributed into paranodes where they colocalized with intact Caspr-labeled axoglial junctions. Furthermore, electron microscopic analysis of the junctions showed intact paranodal septate-like junctions. Thus, the paranodal spectrin-based submembranous cytoskeleton comprises the paranodal barriers required for myelinated axon domain organization.

Introduction

Many cell types are divided into polarized membrane domains with distinct functions. For example, epithelial cells have apical and basal domains with unique protein compositions that facilitate directional transport of molecules. Similarly, neurons are divided into somatodendritic and axonal domains that support directional propagation of action potentials. An even more remarkable example is found in myelinated axons that are further subdivided into functionally and molecularly distinct polarized domains including: (1) nodes of Ranvier characterized by high densities of Na^+ channels, (2) the flanking paranodal junctions where myelin attaches to the axon, and (3) the adjacent juxtaparanodes beneath myelin that are enriched with Kv1 K^+ channels (Poliak and Peles, 2003; Salzer, 2003).

The precise domain organization of myelinated axons depends on neuron–glia interactions. For example, mice with disrupted paranodal junctions have broadened nodal Na^+ channel clusters, Kv1 channels that are located at paranodes rather than beneath the myelin sheath at juxtaparanodes, ataxia, and impaired nerve conduction (Dupree et al., 1999; Bhat et al., 2001; Boyle et al., 2001; Poliak et al., 2001; Rasband et al., 2003; Rios et al., 2003; Pillai et al., 2009). Paranodes function as barriers that exclude Kv1 channels (Pedraza et al., 2001; Rasband, 2004) and are also one of several mechanisms contributing to nodal Na^+ channel clustering during development (Zonta et al., 2008; Feinberg et al., 2010; Susuki et al., 2013).

Despite their importance, how paranodes function as barriers remains unknown. In axons, a submembranous cytoskeleton comprised of ankyrinB, αII spectrin, and βII spectrin can function as a boundary, or barrier, to restrict ankyrinG, the scaffolding protein thought to be responsible for Na^+ channel clustering, to the axon initial segment, a membrane domain that is functionally and molecularly similar to nodes (Garrido et al., 2003; Rasband, 2010; Galiano et al., 2012; Gasser et al., 2012). Intriguingly, paranodes of myelinated axons also have ankyrinB, αII spectrin, and βII spectrin (Ogawa et al., 2006), and these cytoskeletal proteins could function as a cytoskeletal barrier that restricts Na^+ and Kv1 channels to nodes and juxtaparanodes, respectively.

Spectrins form a submembranous cytoskeleton that, together with ankyrins and 4.1 proteins, is thought to link membrane proteins to actin (Bennett and Baines, 2001). Spectrins are comprised of α- and β-subunits that normally form antiparallel heterodimers. Two α- (αI and αII) and five β-subunits (βI–βV) have been cloned in mammals. Increasing evidence suggests spectrins are essential for proper nervous system function. For example, dominant-negative mutations in αII spectrin

Correspondence to Matthew N. Rasband: rasband@bcm.edu

Abbreviations used in this paper: CAM, cell adhesion molecule; DRG, dorsal root ganglion.

The Rockefeller University Press $30.00
J. Cell Biol. Vol. 203 No. 3 437–443
www.jcb.org/cgi/doi/10.1083/jcb.201308116

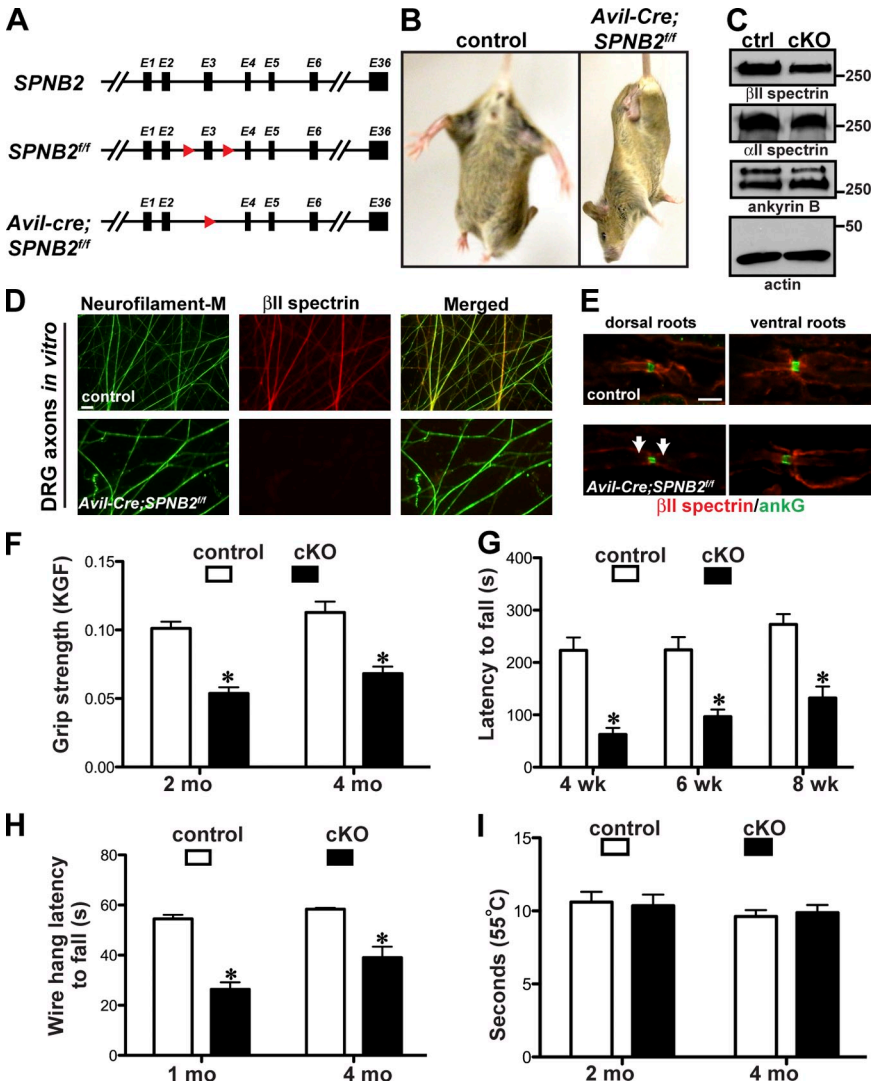

Figure 1. **Generation and characterization of mice lacking βII spectrin in sensory neurons.** (A) Targeting strategy to generate Cre-dependent loss of βII spectrin. (B) Photographs showing control and *Avil-Cre;SPNB2*$^{f/f}$ mice. Mutant mice show a prominent hindlimb clasping phenotype. (C) Immunoblots of dorsal sensory roots from control (ctrl) and *Avil-Cre;SPNB2*$^{f/f}$ (cKO) mice. (D) Immunostaining of cultured DRG axons from control and *Avil-Cre;SPNB2*$^{f/f}$ mice. Axons were stained using antibodies against Neurofilament-M (green) and βII spectrin (red). Bar, 5 µm. (E) Immunostaining of dorsal and ventral roots from control and *Avil-Cre;SPNB2*$^{f/f}$ mice using antibodies against βII spectrin and ankyrinG shows loss of paranodal βII spectrin. Bar, 5 µm. (F) Measurement of grip strength at 2 and 4 mo of age. *Avil-Cre;SPNB2*$^{f/f}$ mice have significantly reduced grip strength compared with control mice. *n* = 19 control, 19 cKO. KGF, kilogram-force. (G) Measurement of latency to fall on an accelerating rotarod. *Avil-Cre;SPNB2*$^{f/f}$ mice perform significantly worse than control mice. *n* = 10 control, 13 cKO. (H) Measurement of latency to fall using the wire-hang test. *Avil-Cre;SPNB2*$^{f/f}$ mice perform significantly worse than control mice. *n* = 15 control, 14 cKO. (I) Measurement of thermal nociception using the hot-plate assay. No difference was observed between control and *Avil-Cre;SPNB2*$^{f/f}$ mice. *n* = 18 control, 18 cKO. Error bars indicate ± SEM. *, P < 0.01.

in humans cause West syndrome with severe cerebral hypomyelination, spastic quadriplegia, and developmental delay (Saitsu et al., 2010; Writzl et al., 2012). Similarly, mice lacking αII or βII spectrin are embryonic lethal, emphasizing the importance of these cytoskeletal proteins (Tang et al., 2003; Stankewich et al., 2011).

Here, we generated mice lacking βII spectrin in peripheral sensory axons to determine if the paranodal spectrin cytoskeleton is the molecular basis of the paranodal barrier. We found that although axoglial junctions remained intact, juxtaparanodal Kv1 channel protein complexes were no longer excluded from paranodes and nodes. Thus, the paranodal spectrin-based cytoskeleton functions as a barrier that restricts axonal membrane proteins to distinct domains.

Results and discussion

Generation of mice with sensory neuron–specific deletion of βII spectrin

To determine if the paranodal cytoskeleton contributes to assembly or function of the paranodal barrier in myelinated axons, and to circumvent the embryonic lethality seen with whole-animal spectrin knockouts, we generated a conditional null mutant allele where exon 3 of the βII spectrin gene (*SPNB2*) is flanked by LoxP sites (*SPNB2*$^{f/f}$ mice) and thus can be deleted in the presence of Cre recombinase (Fig. 1 A; Galiano et al., 2012). We selectively eliminated βII spectrin in peripheral sensory neurons by using Advillin$^{Cre/+}$ (*Avil-Cre*) knock-in mice (Zhou et al., 2010); homozygous conditional knockout mice are referred to as *Avil-Cre;SPNB2*$^{f/f}$ or cKO, and *SPNB2*$^{f/f}$ littermates were used as control mice. The sensory neuron specific cKO mice are an excellent model to study the effects of loss of βII spectrin in axons because myelinated sensory and motor axons from the same mouse can be analyzed by comparing dorsal and ventral roots, respectively. cKO mice were viable, bred normally, groomed well, and showed no difference in size, body weight, or overall appearance compared with controls. However, starting at two weeks of age, cKO mice exhibited significant hind leg clasping (Fig. 1 B). Immunoblots of dorsal roots from control and cKO mice showed only a small decrease in the levels of βII spectrin and αII spectrin, reflecting the high levels of these cytoskeletal proteins expressed in Schwann cells (Fig. 1 C; Susuki et al., 2011). We confirmed the specific deletion of βII spectrin

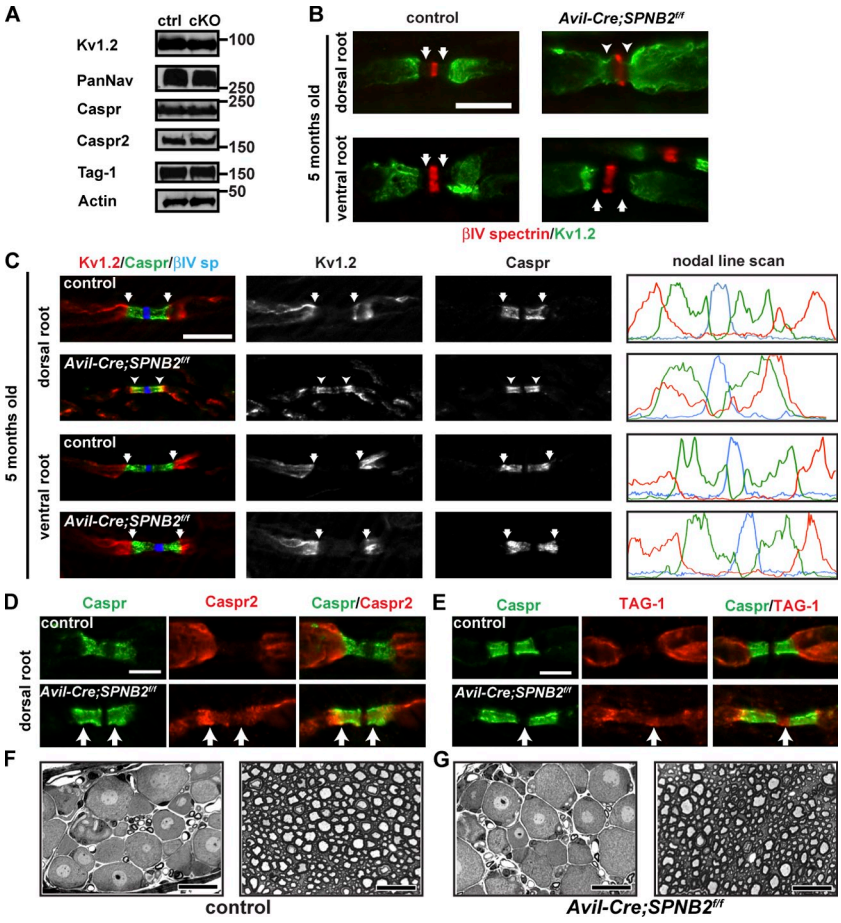

Figure 2. **Loss of βII spectrin disrupts paranodal membrane barriers.** (A) Immunoblot analysis of dorsal roots using antibodies against nodal, paranodal, and juxtaparanodal proteins. (B) Immunostaining of 5-mo-old dorsal and ventral roots from control and *Avil-Cre;SPNB2*$^{f/f}$ mice using antibodies against Kv1.2 and βIV spectrin. Control axons have a pronounced paranodal gap in immunoreactivity between Kv1.2 and βIV spectrin (arrows), but βII spectrin–deficient axons have paranodal Kv1.2 (arrowheads) that is directly adjacent to nodal βIV spectrin staining. Bar, 10 µm. (C) Immunostaining of 5-mo-old dorsal and ventral roots shows overlap between caspr and Kv1.2 in *Avil-Cre;SPNB2*$^{f/f}$ dorsal roots. Line scans of immunofluorescence intensity for the depicted nodes are shown at the right. Kv1.2 is shown in red, caspr in green, and βIV spectrin is shown in blue. Bar, 10 µm. (D) Immunostaining of dorsal roots shows juxtaparanodal Caspr2 (red) is excluded from Caspr-labeled paranodes (green) in control but not *Avil-Cre;SPNB2*$^{f/f}$ (cKO) mice. Bar, 5 µm. (E) Immunostaining of dorsal roots shows juxtaparanodal TAG-1 (red) is excluded from Caspr-labeled paranodes (green) in control but not cKO mice. Instead, TAG-1 can be found at both paranodes and nodes. Bar, 5 µm. (F and G) Toluidine blue–stained dorsal root ganglia and dorsal roots from control (*SPNB2*$^{f/f}$) and *Avil-Cre;SPNB2*$^{f/f}$ mice show no signs of neurodegeneration. Bars, 20 µm.

in sensory neurons by immunostaining cultured dorsal root ganglion (DRG) axons using antibodies against Neurofilament-M and βII spectrin; βII spectrin protein was not detectable in cKO DRG axons (Fig. 1 D). Immunostaining of dorsal and ventral roots from cKO and control mice confirmed the specific elimination of βII spectrin from cKO myelinated sensory axons (Fig. 1 E).

βII spectrin cKO mice have impaired motor coordination

To evaluate the functional consequence of loss of βII spectrin from sensory neurons, we measured dorsal root conduction velocity in 5-wk-old and 1 yr-old mice. Surprisingly, we found no difference between control and cKO mice (5 wk: WT, 7.9 ± 1.3 m/s and cKO 9.5 ± 0.5 m/s; 1 yr: WT, 13.1 ± 1.1 m/s and cKO 12.9 ± 0.7 m/s). Nevertheless, when we performed a series of tests to evaluate motor coordination, thermal nociception, and muscle strength, we observed that at all ages the cKO mice had significantly reduced grip strength (Fig. 1 F) and latency to fall times on rotarod and wire-hang tests (Fig. 1, G and H, respectively) compared with controls. However, we observed no difference in thermal nociception between cKO and control mice using the hot-plate test (Fig. 1 I). Together, these results suggest that thermal nociception, mediated largely by unmyelinated sensory fibers, is not affected by loss of βII spectrin, but information carried by myelinated sensory axons (e.g., proprioception) is significantly affected.

Loss of βII spectrin disrupts membrane domain organization in myelinated axons

We next determined if loss of axonal βII spectrin affects the amount or localization of nodal, paranodal, or juxtaparanodal proteins. Immunoblots showed no difference in the amounts of proteins between dorsal roots from control and cKO mice when probed using antibodies against nodal (PanNav), paranodal (Caspr), or juxtaparanodal (Kv1.2, Caspr2, and Tag-1) proteins (Fig. 2 A). In ventral and control dorsal roots we observed a prominent gap in immunoreactivity between Kv1 channels and nodal βIV spectrin that corresponds to the paranode (Fig. 2 B, arrows). In contrast, immunostaining of βII spectrin–deficient axons showed that Kv1.2 channels, normally restricted to juxtaparanodes, were located in paranodal regions adjacent to the nodes of Ranvier (Fig. 2 B, arrowheads). Immunofluorescence and line scans through ventral and control dorsal root nodes of Ranvier showed sharp transitions in the distributions of juxtaparanodal and paranodal proteins (Fig. 2 C, arrows). Remarkably, dorsal root axons lacking βII spectrin had paranodal Kv1.2 immunoreactivity despite intact Caspr staining (Fig. 2 C, arrowheads). Similar to Kv1.2, other components of the juxtaparanodal K^+ channel complex including Caspr2, TAG-1, and protein 4.1B also redistributed into paranodal (Fig. 2, D and E; protein 4.1B not depicted) and even nodal regions in cKO axons (Fig. 2 E). Interestingly, although ankB is found at paranodes and can bind to βII spectrin (Ogawa et al., 2006), its

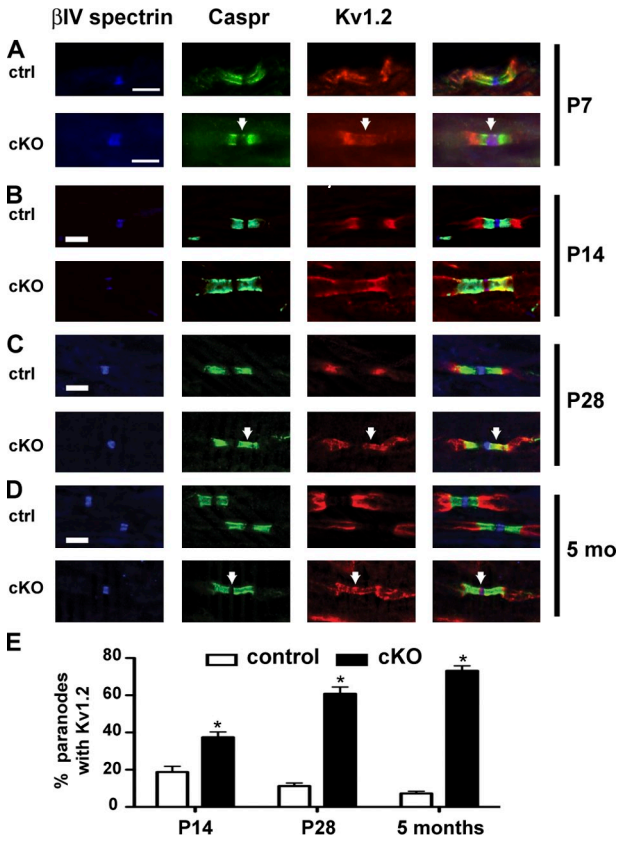

Figure 3. **Paranodal Kv1 K⁺ channel staining increases with age in βII spectrin–deficient axons.** (A–D) Nodes of Ranvier, paranodes, and juxtaparanodes from control (ctrl) and *Avil-Cre;SPNB2$^{f/f}$* (cKO) dorsal roots immunostained using antibodies against βIV spectrin (blue), Caspr (green), and Kv1.2 (red), respectively. Immunostaining was performed at postnatal day P7 (A), P14 (B), P28 (C), and at 5 mo of age (D). Arrows indicate aberrant localization of Kv1.2 in nodes (A and D) and paranodes (B and C). Bars, 5 µm. (E) Quantification of the percentage of paranodes with Kv1.2 immunoreactivity as a function of age. Error bars indicate ± SEM. *, $P < 0.01$.

localization was not affected by loss of axonal βII spectrin (not depicted).

Previously, studies in *C. elegans* showed that loss of β-spectrin causes axon degeneration (Hammarlund et al., 2007). Furthermore, dysmyelination and demyelination can also disrupt juxtaparanodal Kv1 channel localization in axons (Poliak and Peles, 2003). To exclude the possibility that the defects observed in cKO mice are caused by neuron or axon degeneration, dysmyelination, or demyelination, we examined sections of plastic embedded DRG neurons and roots. We found no signs of neuronal or axonal degeneration, and no indication of dys- or demyelination (Fig. 2, F and G). Together, these results suggest that the molecular basis of the paranodal barrier is the βII spectrin–dependent submembranous cytoskeleton.

βII spectrin is required for maintenance of membrane domains in myelinated axons

The initial assembly of juxtaparanodal, paranodal, and nodal domains in the PNS is thought to depend on interactions between membrane-associated cell adhesion molecules (CAMs; Schafer and Rasband, 2006). For example, juxtaparanodal clustering of Kv1 channels requires trans-interactions between axonal Caspr2 and glial TAG-1, and genetic deletion of either CAM blocks channel clustering (Poliak et al., 2003; Traka et al., 2003). At paranodes, clustering of βII spectrin may depend on Caspr, because Caspr has a cytoplasmic protein 4.1 binding domain, protein 4.1B binds to βII spectrin, and all three proteins are found at paranodes (Ogawa et al., 2006). To determine if paranodal βII spectrin is required for the maintenance of axonal membrane domains, we analyzed Kv1.2 localization in myelinated axons throughout development and into adulthood. As previously reported (Vabnick et al., 1999), we found Kv1.2 immunoreactivity colocalized with paranodal Caspr during the first postnatal week (unpublished data). However, as early as P7 we found instances of aberrant localization of Kv1.2 in cKO myelinated dorsal root axons, including at nodes of Ranvier (Fig. 3 A, arrow). By two weeks of age in control mice, fewer than 20% of paranodes had detectable Kv1.2 immunoreactivity, and this continued to decrease as mice matured (Fig. 3, B–E). In contrast, at two weeks nearly 40% of paranodes in cKO dorsal root axons had detectable Kv1.2 (Fig. 3, B and E), and the frequency of paranodal Kv1.2 continued to increase as cKO mice aged; in 5 mo-old cKO mice nearly 80% of paranodes had detectable Kv1.2 (Fig. 3, D and E). Furthermore, nodal Kv1.2 was often detected in adult cKO dorsal root axons, but was never seen in control mice (Fig. 3 D, arrow). The consistent increase in the number of paranodes with Kv1.2 immunoreactivity with increasing age suggests that βII spectrin plays important rolefor the maintenance of myelinated axon membrane domain organization.

Loss of βII spectrin does not disrupt paranodal ultrastructure or axon–glia interactions in the PNS

The formation of membrane domains along axons is thought to depend on the septate-like junctions found at paranodes (Rosenbluth, 2009). To determine if these axoglial junctions are intact in axons lacking βII spectrin, we performed electron microscopic analyses of longitudinal sections of myelinated axons from control and cKO adult dorsal roots. We found that in both genotypes the paranodal myelin loops and the nodal domains were well preserved, despite a widened node in the cKO (Fig. 4 A). Remarkably, close examination of the paranodes in cKO roots also revealed transverse bands (Fig. 4 B, arrowheads), a hallmark of intact septate-like, paranodal junctions (Mierzwa et al., 2010). Thus, in βII spectrin cKO mice, Kv1 channels enter into nodal and paranodal domains despite normal myelination and intact paranodal junctions, including transverse bands.

Although paranodes formed properly and had intact transverse bands, 5-mo-old mice lacking βII spectrin in sensory neurons had, on average, nodal Na^+ channel clusters that were more than twice the length of nodes from control mice and cKO ventral roots (Fig. 4, C and D). Even at one year of age paranodal junctions, defined by Caspr staining, in βII spectrin–deficient axons remained intact and indistinguishable from ventral or control dorsal root axons (Fig. 4 E), although nodes were still longer (Fig. 4 F). The broadening of nodal Na^+ channels and redistribution of juxtaparanodal Kv1 channel complexes is remarkably

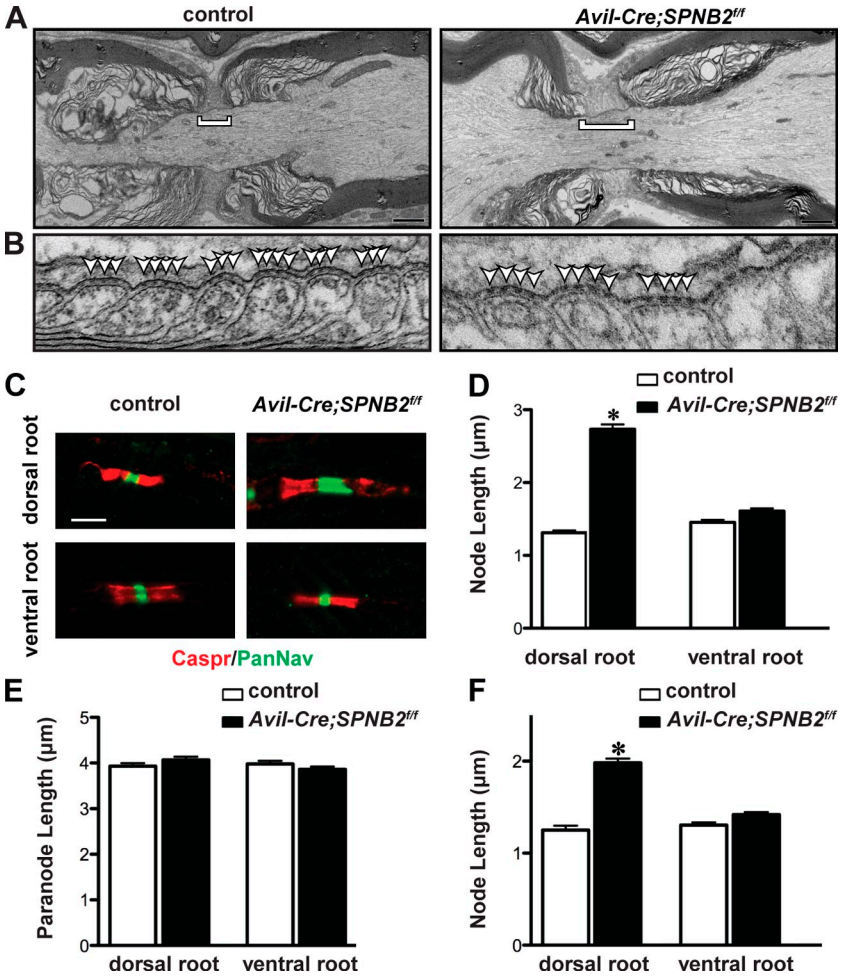

Figure 4. **βII spectrin–deficient PNS axons have intact paranodal junctions and transverse bands.** (A and B) Electron microscopy of dorsal root nodes of Ranvier from control and *Avil-Cre;SPNB2$^{f/f}$* mice. Mutant mice have widened nodes (brackets), but intact transverse bands (white arrowheads). Bar, 1 µm. (C) Immunostaining of control and *Avil-Cre;SPNB2$^{f/f}$* dorsal and ventral roots using antibodies against Caspr (red) and Na^+ channels (PanNav; green). Bar, 3 µm. (D) Quantification of node length in 5-mo-old dorsal and ventral roots. Error bars indicate ± SEM. *, $P < 0.01$. $n = 4$ control, 4 cKO. A total of 132 nodes were counted for control dorsal and ventral roots, and cKO ventral roots. A total of 124 nodes were counted for cKO dorsal roots. (E and F) Quantification of paranode and node length in 1-yr-old dorsal and ventral roots. No difference was observed in paranode length, but node length was significantly increased. Error bars indicate ± SEM, *, $P < 0.01$. $n = 4$ control, 4 cKO. A total of 100 nodes and 100 paranodes were counted for each genotype.

similar to the alterations in axon domain organization observed previously in mice with frank disruption of paranodal axoglial junctions due to genetic deletion of Caspr, contactin, or NF-155, the cell adhesion molecules that mediate paranodal axoglial interactions (Bhat et al., 2001; Boyle et al., 2001; Pillai et al., 2009).

The major observation in this study is that juxtaparanodal proteins are mislocalized and found at paranodes in axons lacking βII spectrin despite an intact paranodal junction. This observation leads to the important conclusion that spectrin-based cytoskeletons participate in the assembly and maintenance of polarized cellular domains, including myelinated axon domain organization. Furthermore, the results reported here support the notion that the βII spectrin–based cytoskeleton functions as a repeating intra-axonal boundary that restricts membrane proteins, including ion channels and cell adhesion molecules, to juxtaparanodes and nodes, a characteristic of the axonal cytoskeleton that was recently shown to contribute to Na^+ channel clustering at axon initial segments (Galiano et al., 2012). Because nodes of Ranvier are thought to be evolutionarily derived from axon initial segments (Hill et al., 2008), it is not surprising that similar mechanisms of assembly would exist for each of these important excitable domains. Nevertheless, there are also important differences in how these barrier cytoskeletons are assembled. For instance, the formation of the intra-axonal boundary contributing to ankG clustering at the AIS requires neither myelination nor any other extrinsic factor or interaction. In contrast, the clustering of nodal Na^+ channels and juxtaparanodal K^+ channels requires myelination and neuron–glia interactions, indicating that glial cells orchestrate the assembly of the paranodal submembranous spectrin cytoskeleton.

The role of the paranode as a membrane barrier and contributor to node formation is controversial (Thaxton et al., 2011). For example, if paranodes and paranodal cytoskeletons are so important to axon domain organization, why is there not a more significant effect on nodal Na^+ channel clustering in mutants that lack appropriate paranodal junctions (e.g., Caspr, contactin, and NF-155 mutants)? Recent studies have answered this question by showing that there exist multiple, overlapping mechanisms contributing to Na^+ channel clustering in the PNS and CNS so that loss of only one mechanism (i.e., the paranodal barrier mechanism) does not inhibit node formation (Zonta et al., 2008; Feinberg et al., 2010; Susuki et al., 2013).

How might the paranodal cytoskeleton function as a barrier? We speculate that the paranodal spectrin-based cytoskeleton functions as a general membrane barrier, limiting the lateral diffusion of all axolemmal membrane proteins to distinct domains. However, the effectiveness of this barrier may depend on the size and/or composition of the entire protein complex rather than just a single membrane protein. For example, juxtaparanodal

Kv1 channels are part of a larger protein complex that also includes Caspr2, ADAM22, PSD-93/95, and protein 4.1B. Together, these cytoplasmic scaffolds and membrane proteins are unable to bypass the paranodal cytoskeleton. Additional specification for location in the axonal membrane depends on neuron–glia interactions. Thus, the cytoskeletal membrane boundary and neuron–glia interactions normally work together to organize distinct membrane domains along myelinated axons.

Surprisingly, despite paranodal Kv1 channels, compound action potentials in the βII spectrin cKO mice were indistinguishable from control mice and showed no difference in conduction velocity. In contrast, paranodal mutant mice (e.g., Caspr, contactin, and NF-155 knockouts) lacking axon–glia interactions and transverse bands have significant slowing of nerve conduction (Bhat et al., 2001; Boyle et al., 2001; Pillai et al., 2009). This difference emphasizes the role of the paranodal junction itself for normal nerve conduction and supports the idea that paranodal junctions also limit the activity of the Kv1 channels located beneath the overlying myelinating Schwann cell. The results reported here support the conclusion that paranodes function as membrane barriers, and demonstrate a surprising molecular mechanism that depends on the spectrin-based paranodal cytoskeleton rather than exclusive interactions between axonal and glial cell adhesion molecules.

Materials and methods

Mice

Generation of conditional alleles for *Spnb2* was achieved by flanking exon3 with loxP sites. Upon Cre-mediated recombination the reading frame is disrupted, resulting in a truncated transcript (Galiano et al., 2012). The *Spnb2* floxed mice were maintained on a mixed C57BL/6 and 129/Sv background. *Avil-Cre* mice were provided by F. Wang (Duke University, Durham, NC). All experiments were performed in compliance with the National Institutes of Health Guide for the Care and Use of Laboratory Animals and were approved by the Baylor College of Medicine Institutional Animal Care and Use Committee.

Antibodies

The mouse pan anti-Na^+ channel (pan Nav; Sigma-Aldrich) and Rabbit anti-Kv1.2 (generated against the peptide GVNNSNEDFREENLKTAN found in the C-terminal cytoplasmic domain), anti-Caspr (generated against a GST fusion protein containing the cytoplasmic domain of Caspr), anti-4.1B (generated against a fusion protein containing amino acids 778–968 of human 4.1B), and anti-βIV spectrin (generated against the peptide sequence DRAEELPRRRRPERQE found in the C-terminal "specific domain") antibodies have been described previously (Schafer et al., 2004; Ogawa et al., 2006, 2008). Rabbit polyclonal antibodies against neurofilament M and mouse monoclonal actin (clone C4) antibody were purchased from EMD Millipore. Mouse monoclonal antibodies against ankyrinB (N105/17) and ankyrinG (N106/36) were purchased from the UC Davis/NIH NeuroMab Facility (Davis, CA). Mouse monoclonal antibodies against βII spectrin were purchased from BD. Rabbit polyclonal antibodies specific for Caspr2 were purchased from Abcam and anti–contactin-2/TAG1 was purchased from R&D Systems. Alexa Fluor 350, 488, and 594 secondary antibodies were purchased from Invitrogen.

Immunofluorescence and electron microscopy

Immunostaining of spinal dorsal and ventral roots was performed as described previously (Ogawa et al., 2006). In brief, roots were dissected, fixed in 4% paraformaldehyde, cryoprotected in 20% sucrose, and then sectioned and placed on coverslips. Sections were permeabilized using 0.3% Triton X-100, and primary antibodies were added overnight. After washing the tissue, secondary antibodies were added for 1 h. Sections were then washed again, air dried, and mounted for visualization on a microscope. All images were acquired using a fluorescence microscope (Imager Z1; Carl Zeiss) fitted with a camera (AxioCam Mrm; Carl Zeiss). Microscope objectives used in this study included 20× (0.8 NA) air, 40× (0.75 NA) air, and 63× (1.4 NA) oil objectives. Image analysis was performed using AxioVision software (Carl Zeiss), and figures were cropped and assembled using Adobe Photoshop and Adobe Illustrator. For electron microscopy, tissues were prepared and processed as described previously (Chang et al., 2010). In brief, mice were anesthetized and then perfused with 2.5% glutaraldehyde and 2.0% paraformaldehyde in 0.1 M cacodylate buffer, pH 7.4. Dorsal roots were dissected and then post-fixed for 3 h. Nerves were then dehydrated and embedded in resin (Electron Microscopy Sciences). The tissues were stained using saturated uranyl acetate plus 50% ethanol during dehydration.

Electrophysiology

CAP recordings of dorsal and ventral roots were performed as described elsewhere (Rasband et al., 1999; Susuki et al., 2013). In brief, roots were acutely dissected and placed in a continuously perfused recording chamber. Each end of the root was drawn into a suction electrode and after stimulation responses were recorded. Conduction velocities were calculated by measuring the length of the nerve and dividing this by the latency from stimulation to the peak of the CAP.

DRG cultures

DRGs were isolated from newly born control and cKO mice. After dissociation by trypsinization and trituration, cells were plated onto coverslips treated with Matrigel and maintained in neurobasal medium supplement with 2% B27, 100 ng/ml NGF, and 1% glutamax. The medium was changed every other day. To eliminate fibroblasts and Schwann cells, cells were treated with 10 µM FUDR (fluorodeoxyuridine; Sigma-Aldrich) in medium for 2 d. Two cycles of FUDR treatment (2 d with FUDR, 2 d without FUDR) were performed to obtain neuron-only cultures. 2-wk-old cultures were fixed for immunostaining.

SDS-PAGE and immunoblotting

Nerve roots were dissected and immediately frozen on dry ice. Tissues were extracted in reducing sample buffer by sonicating on ice, with four on/off cycles of 1 min. Proteins were separated by SDS-PAGE and blotted onto nitrocellulose membranes. Blots were probed with different antibodies as described previously (Schafer et al., 2004).

Behavior analysis

Motor coordination and balance were tested on an accelerating rod (Ugo Basile). In brief, mice were placed on a rotating rod (3-cm diameter) and the time each animal was able to stay on the rod was measured. The rotarod's speed increased from 4 to 40 rpm over a 5-min period. Mice were pretrained for one trial on the accelerating rod before the test. We measured neuromuscular function using a grip-strength meter (Columbus Instruments). Mice were held by the tail, lowered toward the meter, allowed to grasp a metal rod, and then pulled horizontally away from the rod. The force on the bar when the grasp was released was recorded as the grip strength. As another measure of strength and proprioception, mice were placed on top of a metal screen and allowed to accommodate for 3–5 s before the mesh was inverted and held at least 35 cm over a mouse cage containing 5–7 cm of soft bedding. The latency to completely fall from the mesh was recorded; the cutoff time was 60 s, after which mice were immediately returned to their home cage. As a measure of thermal nociception, mice were placed on a plate maintained at 55.0°C (Columbus Instruments). The latency to respond to the heat stimulus was measured and recorded. Mice remained on the plate until they performed one of the following behaviors regarded as indicative of a nociceptive heat response: paw lick, paw shake, or jump. The cutoff time was set at 30 s. In the absence of a reflex response within 30 s, the mouse was removed from the hot plate to avoid tissue damage.

This work was supported by National Institutes of Health grants (NS069688 and NS044916 to M.N. Rasband), the National Multiple Sclerosis Society, and the Dr. Miriam and Sheldon Adelson Medical Research Foundation.

The authors declare no competing interests.

Submitted: 20 August 2013
Accepted: 26 September 2013

References

Bennett, V., and A.J. Baines. 2001. Spectrin and ankyrin-based pathways: metazoan inventions for integrating cells into tissues. *Physiol. Rev.* 81: 1353–1392.

Bhat, M.A., J.C. Rios, Y. Lu, G.P. Garcia-Fresco, W. Ching, M. St Martin, J. Li, S. Einheber, M. Chesler, J. Rosenbluth, et al. 2001. Axon-glia interactions and the domain organization of myelinated axons requires

neurexin IV/Caspr/Paranodin. *Neuron*. 30:369–383. http://dx.doi.org/10.1016/S0896-6273(01)00294-X

Boyle, M.E., E.O. Berglund, K.K. Murai, L. Weber, E. Peles, and B. Ranscht. 2001. Contactin orchestrates assembly of the septate-like junctions at the paranode in myelinated peripheral nerve. *Neuron*. 30:385–397. http://dx.doi.org/10.1016/S0896-6273(01)00296-3

Chang, K.J., K. Susuki, M.T. Dours-Zimmermann, D.R. Zimmermann, and M. N. Rasband. 2010. Oligodendrocyte myelin glycoprotein does not influence node of ranvier structure or assembly. *J. Neurosci.* 30:14476–14481. http://dx.doi.org/10.1523/JNEUROSCI.1698-10.2010

Dupree, J.L., J.-A. Girault, and B. Popko. 1999. Axo-glial interactions regulate the localization of axonal paranodal proteins. *J. Cell Biol.* 147:1145–1152. http://dx.doi.org/10.1083/jcb.147.6.1145

Feinberg, K., Y. Eshed-Eisenbach, S. Frechter, V. Amor, D. Salomon, H. Sabanay, J.L. Dupree, M. Grumet, P.J. Brophy, P. Shrager, and E. Peles. 2010. A glial signal consisting of gliomedin and NrCAM clusters axonal Na+ channels during the formation of nodes of Ranvier. *Neuron*. 65:490–502. http://dx.doi.org/10.1016/j.neuron.2010.02.004

Galiano, M.R., S. Jha, T.S. Ho, C. Zhang, Y. Ogawa, K.J. Chang, M.C. Stankewich, P.J. Mohler, and M.N. Rasband. 2012. A distal axonal cytoskeleton forms an intra-axonal boundary that controls axon initial segment assembly. *Cell*. 149:1125–1139. http://dx.doi.org/10.1016/j.cell.2012.03.039

Garrido, J.J., P. Giraud, E. Carlier, F. Fernandes, A. Moussif, M.P. Fache, D. Debanne, and B. Dargent. 2003. A targeting motif involved in sodium channel clustering at the axonal initial segment. *Science*. 300:2091–2094. http://dx.doi.org/10.1126/science.1085167

Gasser, A., T.S.-Y. Ho, X. Cheng, K.J. Chang, S.G. Waxman, M.N. Rasband, and S.D. Dib-Hajj. 2012. An ankyrinG-binding motif is necessary and sufficient for targeting Nav1.6 sodium channels to axon initial segments and nodes of Ranvier. *J. Neurosci.* 32:7232–7243. http://dx.doi.org/10.1523/JNEUROSCI.5434-11.2012

Hammarlund, M., E.M. Jorgensen, and M.J. Bastiani. 2007. Axons break in animals lacking beta-spectrin. *J. Cell Biol.* 176:269–275. http://dx.doi.org/10.1083/jcb.200611117

Hill, A.S., A. Nishino, K. Nakajo, G. Zhang, J.R. Fineman, M.E. Selzer, Y. Okamura, and E.C. Cooper. 2008. Ion channel clustering at the axon initial segment and node of Ranvier evolved sequentially in early chordates. *PLoS Genet.* 4:e1000317. http://dx.doi.org/10.1371/journal.pgen.1000317

Mierzwa, A.J., J.C. Arevalo, R. Schiff, M.V. Chao, and J. Rosenbluth. 2010. Role of transverse bands in maintaining paranodal structure and axolemmal domain organization in myelinated nerve fibers: effect on longevity in dysmyelinated mutant mice. *J. Comp. Neurol.* 518:2841–2853.

Ogawa, Y., D.P. Schafer, I. Horresh, V. Bar, K. Hales, Y. Yang, K. Susuki, E. Peles, M.C. Stankewich, and M.N. Rasband. 2006. Spectrins and ankyrinB constitute a specialized paranodal cytoskeleton. *J. Neurosci.* 26:5230–5239. http://dx.doi.org/10.1523/JNEUROSCI.0425-06.2006

Ogawa, Y., I. Horresh, J.S. Trimmer, D.S. Bredt, E. Peles, and M.N. Rasband. 2008. Postsynaptic density-93 clusters Kv1 channels at axon initial segments independently of Caspr2. *J. Neurosci.* 28:5731–5739. http://dx.doi.org/10.1523/JNEUROSCI.4431-07.2008

Pedraza, L., J.K. Huang, and D.R. Colman. 2001. Organizing principles of the axoglial apparatus. *Neuron*. 30:335–344. http://dx.doi.org/10.1016/S0896-6273(01)00306-3

Pillai, A.M., C. Thaxton, A.L. Pribisko, J.G. Cheng, J.L. Dupree, and M.A. Bhat. 2009. Spatiotemporal ablation of myelinating glia-specific neurofascin (Nfasc NF155) in mice reveals gradual loss of paranodal axoglial junctions and concomitant disorganization of axonal domains. *J. Neurosci. Res.* 87:1773–1793. http://dx.doi.org/10.1002/jnr.22015

Poliak, S., and E. Peles. 2003. The local differentiation of myelinated axons at nodes of Ranvier. *Nat. Rev. Neurosci.* 4:968–980. http://dx.doi.org/10.1038/nrn1253

Poliak, S., L. Gollan, D. Salomon, E.O. Berglund, R. Ohara, B. Ranscht, and E. Peles. 2001. Localization of Caspr2 in myelinated nerves depends on axon-glia interactions and the generation of barriers along the axon. *J. Neurosci.* 21:7568–7575.

Poliak, S., D. Salomon, H. Elhanany, H. Sabanay, B. Kiernan, L. Pevny, C.L. Stewart, X. Xu, S.Y. Chiu, P. Shrager, et al. 2003. Juxtaparanodal clustering of Shaker-like K+ channels in myelinated axons depends on Caspr2 and TAG-1. *J. Cell Biol.* 162:1149–1160. http://dx.doi.org/10.1083/jcb.200305018

Rasband, M.N. 2004. It's "juxta" potassium channel! *J. Neurosci. Res.* 76:749–757. http://dx.doi.org/10.1002/jnr.20073

Rasband, M.N. 2010. The axon initial segment and the maintenance of neuronal polarity. *Nat. Rev. Neurosci.* 11:552–562. http://dx.doi.org/10.1038/nrn2852

Rasband, M.N., E. Peles, J.S. Trimmer, S.R. Levinson, S.E. Lux, and P. Shrager. 1999. Dependence of nodal sodium channel clustering on paranodal axoglial contact in the developing CNS. *J. Neurosci.* 19:7516–7528.

Rasband, M.N., C.M. Taylor, and R. Bansal. 2003. Paranodal transverse bands are required for maintenance but not initiation of Nav1.6 sodium channel clustering in CNS optic nerve axons. *Glia*. 44:173–182. http://dx.doi.org/10.1002/glia.10284

Rios, J.C., M. Rubin, M. St Martin, R.T. Downey, S. Einheber, J. Rosenbluth, S.R. Levinson, M. Bhat, and J.L. Salzer. 2003. Paranodal interactions regulate expression of sodium channel subtypes and provide a diffusion barrier for the node of Ranvier. *J. Neurosci.* 23:7001–7011.

Rosenbluth, J. 2009. Multiple functions of the paranodal junction of myelinated nerve fibers. *J. Neurosci. Res.* 87:3250–3258. http://dx.doi.org/10.1002/jnr.22013

Saitsu, H., J. Tohyama, T. Kumada, K. Egawa, K. Hamada, I. Okada, T. Mizuguchi, H. Osaka, R. Miyata, T. Furukawa, et al. 2010. Dominant-negative mutations in alpha-II spectrin cause West syndrome with severe cerebral hypomyelination, spastic quadriplegia, and developmental delay. *Am. J. Hum. Genet.* 86:881–891. http://dx.doi.org/10.1016/j.ajhg.2010.04.013

Salzer, J.L. 2003. Polarized domains of myelinated axons. *Neuron*. 40:297–318. http://dx.doi.org/10.1016/S0896-6273(03)00628-7

Schafer, D.P., and M.N. Rasband. 2006. Glial regulation of the axonal membrane at nodes of Ranvier. *Curr. Opin. Neurobiol.* 16:508–514. http://dx.doi.org/10.1016/j.conb.2006.08.003

Schafer, D.P., R. Bansal, K.L. Hedstrom, S.E. Pfeiffer, and M.N. Rasband. 2004. Does paranode formation and maintenance require partitioning of neurofascin 155 into lipid rafts? *J. Neurosci.* 24:3176–3185. http://dx.doi.org/10.1523/JNEUROSCI.5427-03.2004

Stankewich, M.C., C.D. Cianci, P.R. Stabach, L. Ji, A. Nath, and J.S. Morrow. 2011. Cell organization, growth, and neural and cardiac development require αII-spectrin. *J. Cell Sci.* 124:3956–3966. http://dx.doi.org/10.1242/jcs.080374

Susuki, K., A.R. Raphael, Y. Ogawa, M.C. Stankewich, E. Peles, W.S. Talbot, and M.N. Rasband. 2011. Schwann cell spectrins modulate peripheral nerve myelination. *Proc. Natl. Acad. Sci. USA*. 108:8009–8014. http://dx.doi.org/10.1073/pnas.1019600108

Susuki, K., K.J. Chang, D.R. Zollinger, Y. Liu, Y. Ogawa, Y. Eshed-Eisenbach, M.T. Dours-Zimmermann, J.A. Oses-Prieto, A.L. Burlingame, C.I. Seidenbecher, et al. 2013. Three mechanisms assemble central nervous system nodes of Ranvier. *Neuron*. 78:469–482. http://dx.doi.org/10.1016/j.neuron.2013.03.005

Tang, Y., V. Katuri, A. Dillner, B. Mishra, C.X. Deng, and L. Mishra. 2003. Disruption of transforming growth factor-beta signaling in ELF beta-spectrin-deficient mice. *Science*. 299:574–577. http://dx.doi.org/10.1126/science.1075994

Thaxton, C., A.M. Pillai, A.L. Pribisko, J.L. Dupree, and M.A. Bhat. 2011. Nodes of Ranvier act as barriers to restrict invasion of flanking paranodal domains in myelinated axons. *Neuron*. 69:244–257. http://dx.doi.org/10.1016/j.neuron.2010.12.016

Traka, M., L. Goutebroze, N. Denisenko, M. Bessa, A. Nifli, S. Havaki, Y. Iwakura, F. Fukamauchi, K. Watanabe, B. Soliven, et al. 2003. Association of TAG-1 with Caspr2 is essential for the molecular organization of juxtaparanodal regions of myelinated fibers. *J. Cell Biol.* 162:1161–1172. http://dx.doi.org/10.1083/jcb.200305078

Vabnick, I., J.S. Trimmer, T.L. Schwarz, S.R. Levinson, D. Risal, and P. Shrager. 1999. Dynamic potassium channel distributions during axonal development prevent aberrant firing patterns. *J. Neurosci.* 19:747–758.

Writzl, K., Z.R. Primec, B.G. Stražišar, D. Osredkar, N. Pečarič-Meglič, B.S. Kranjc, K. Nishiyama, N. Matsumoto, and H. Saitsu. 2012. Early onset West syndrome with severe hypomyelination and coloboma-like optic discs in a girl with SPTAN1 mutation. *Epilepsia*. 53:e106–e110. http://dx.doi.org/10.1111/j.1528-1167.2012.03437.x

Zhou, X., L. Wang, H. Hasegawa, P. Amin, B.X. Han, S. Kaneko, Y. He, and F. Wang. 2010. Deletion of PIK3C3/Vps34 in sensory neurons causes rapid neurodegeneration by disrupting the endosomal but not the autophagic pathway. *Proc. Natl. Acad. Sci. USA*. 107:9424–9429. http://dx.doi.org/10.1073/pnas.0914725107

Zonta, B., S. Tait, S. Melrose, H. Anderson, S. Harroch, J. Higginson, D.L. Sherman, and P.J. Brophy. 2008. Glial and neuronal isoforms of Neurofascin have distinct roles in the assembly of nodes of Ranvier in the central nervous system. *J. Cell Biol.* 181:1169–1177. http://dx.doi.org/10.1083/jcb.200712154